Cycling between growth and production phases increases cyanobacteria bioproduction of lactate

Shabestary, K.; Hernández, H.P.; Miao, R.; Ljungqvist, E.; Hallman, O.; Sporre, Emil; Branco Dos Santos, F.; Hudson, E.P.

DOI
10.1016/j.ymben.2021.09.010

Publication date
2021

Document Version
Final published version

Published in
Metabolic Engineering

Metabolic Engineering 68 (2021) 131–141

Contents lists available at ScienceDirect

Metabolic Engineering

journal homepage: www.elsevier.com/locate/meteng

Cycling between growth and production phases increases cyanobacteria bioproduction of lactate

Kiyan Shabestary [a,1], Hugo Pineda Hernández [b], Rui Miao [a], Emil Ljungqvist [a], Olivia Hallman [a], Emil Sporre [a], Filipe Branco dos Santos [b], Elton P. Hudson [a,*]

[a] School of Engineering Sciences in Chemistry, Biotechnology and Health, Science for Life Laboratory, KTH - Royal Institute of Technology, Stockholm, Sweden
[b] Molecular Microbial Physiology Group, Swammerdam Institute for Life Sciences, Faculty of Science, University of Amsterdam, Science Park 904, Amsterdam, 1098 XH, the Netherlands

ARTICLE INFO

Keywords:
Two-stage production
Cyanobacteria
Stress response
Synthetic biology

ABSTRACT

Decoupling growth from product synthesis is a promising strategy to increase carbon partitioning and maximize productivity in cell factories. However, reduction in both substrate uptake rate and metabolic activity in the production phase are an underlying problem for upscaling. Here, we used CRISPR interference to repress growth in lactate-producing *Synechocystis* sp. PCC 6803. Carbon partitioning to lactate in the production phase exceeded 90%, but CO_2 uptake was severely reduced compared to uptake during the growth phase. We characterized strains during the onset of growth arrest using transcriptomics and proteomics. Multiple genes involved in ATP homeostasis were regulated once growth was inhibited, which suggests an alteration of energy charge that may lead to reduced substrate uptake. In order to overcome the reduced metabolic activity and take advantage of increased carbon partitioning, we tested a novel production strategy that involved alternating growth arrest and recovery by periodic addition of an inducer molecule to activate CRISPRi. Using this strategy, we maintained lactate biosynthesis in *Synechocystis* for 30 days in a constant light turbidostat cultivation. Cumulative lactate titers were also increased by 100% compared to a constant growth-arrest regime, and reached 1 g/L. Further, the cultivation produced lactate for 30 days, compared to 20 days for the non-growth arrest cultivation. Periodic growth arrest could be applicable for other products, and in cyanobacteria, could be linked to internal circadian rhythms that persist in constant light.

1. Introduction

The refinement of tight and inducible gene expression tools for a range of microbes has made it possible to implement genetically encoded dynamic modulation of enzyme activity in cell factories. The ability to precisely control gene expression, particularly of a production pathway, can have benefits for process titers and stability (Brockman and Prather, 2015; Lynch, 2016; Venayak et al., 2015). In an ideal dynamic bioprocess, cells grow rapidly to a suitable density and are then switched to a production phase, where the product synthesis pathway is activated and flux to biomass is restricted. A two-phase production that separates growth and product formation can prevent imbalances in metabolic intermediates as well as suboptimal carbon and energy yields that can arise when cells synthesize product and biomass simultaneously (Dunlop et al., 2010; Gadkar et al., 2005; Lo et al., 2016; Shabestary and Hudson, 2016). Two-stage bioproduction can also be more stable than one-stage processes. As the growth phase would not have ongoing product synthesis, selection for faster growing revertants is reduced, and because the production phase restricts cell growth, revertants are less likely to overtake cultures. For cyanobacteria, where cultivation of production strains for several weeks is common, genetic instability of the population (i.e., non-productive mutants overtaking the cultures) is a large hurdle for scale up (Du et al., 2017, 2018; Jones, 2014). Further, controlling cell density also can allow increased substrate or oxygen transfer rates within the bioprocess.

A major limitation of two-stage bioproductions is that the production phase has lower metabolic activity than the growth phase, since supposedly substrate uptake is linked to cellular growth through variable and largely unknown regulatory schemes. The most common method of growth arrest in two-stage processes is limitation of an essential

* Corresponding author. KTH Royal Institute of Technology, Stockholm, Sweden.
E-mail address: paul.hudson@scilifelab.se (E.P. Hudson).
[1] Present address: Department of Bioengineering, Faculty of Engineering, Imperial College London, London, United Kingdom.

https://doi.org/10.1016/j.ymben.2021.09.010
Received 22 June 2021; Received in revised form 3 September 2021; Accepted 25 September 2021
Available online 1 October 2021

nutrient, so that cells enter a stationary phase. A systematic study of *Escherichia coli* and *Bacillus subtilis* substrate uptake rates 48 h into stationary phase showed that substrate uptake was reduced by 50–95%, depending on which nutrient was exhausted (Chubukov and Sauer, 2014). Among photosynthetic cell factories, prominent examples are nitrogen limitation of microalgae, which leads to growth arrest and an increase in lipid biosynthesis as proteins are catabolized (Ho et al., 2012), and nitrogen limitation of the cyanobacterium *Synechocystis*, which results in PHB accumulation (Koch et al., 2020). However, nitrogen limitation stress reduces photosynthetic efficiency and the rate of CO_2 fixation is reduced. The tradeoff between lipid accumulation and cell growth to increase total productivity in microalgae can be optimized through manipulation of nitrogen in the culture media (Adams et al., 2013), and a partial genetic restriction of nitrogen uptake by mutation of a transcription factor increased lipid synthesis in nitrogen replete conditions without compromising CO_2 uptake (Ajjawi et al., 2017).

As an alternative to nutrient limitation, the transition between growth and production phases can be achieved in nutrient replete conditions through a genetic circuit acting on a growth-essential reaction. Such circuits can be composed of synthetic biology parts (Farmer and Liao, 2000). A signal such as metabolite accumulation can activate a controller, such as a transcription factor, which transduces the sensor status to alter expression of the critical gene. There are numerous examples of growth-production control systems implemented in microbes, where the controller can act on the valve at the level of transcription (Landberg et al., 2020; Wu et al., 2021; Li et al., 2016; Soma et al., 2014; Shabestary et al., 2018), translation (Abramson et al., 2018; Solomon et al., 2012), or post-translationally (Durante-Rodríguez et al., 2018; Schramm et al., 2020).

Genetic growth-arrest systems have also been demonstrated in cyanobacteria. Inducible, CRISPRi-based repression of *odhB* (a subunit of the pyruvate dehydrogenase complex) and *gltA* (citrate synthase), arrested growth and increased specific productivity of ethanol, and n-butanol, respectively (Shabestary et al., 2018). This strategy targeted competing metabolic pathways that were also essential for growth. In an alternative approach, IPTG-induced expression of the transcription factor RpaB arrested growth in *Synechococcus* PCC 7942, which led to increased specific productivity of sucrose compared to control strain where RpaB was not overexpressed (Abramson et al., 2018). In both cases, the growth arrest led to reduced metabolic activity. Repression of *odhB* and *gltA* reduced CO_2 fixation by 75% at 5 d. RpaB overexpression decreased photosynthetic efficiency from 0.25 at 1 d to 0.1 at 4 d post-induction. In both reports, metabolic activity was reduced despite abundant CO_2 and light, though the mechanisms were not elucidated. To realize the potential of dynamic metabolic engineering, it is important to investigate the mechanisms for reduced metabolic activity when growth is arrested, as well as to develop genetic or process engineering strategies to keep metabolic rates high.

Here, we characterized lactate-producing *Synechocystis* cultures that were growth arrested by CRISPRi of the essential enzyme citrate synthase. The *Synechocystis* citrate synthase has been recently characterized (Ito et al., 2019). The stoichiometry of the cyanobacterial enzyme is not known, but is presumed to assemble as a homo-multimer, as the *E. coli* enzyme is a homo-hexamer, so that only one gene is targeted for repression (*gltA*). The *Synechocystis* citrate synthase catalyzes synthesis of citrate and not cleavage, and has relatively slow kinetics compared to other bacterial citrate synthases. Repression of citrate synthase increases specific productivity as well as total titers of lactate, but CO_2 uptake is reduced after a few days. Growth could be recovered by addition of glutamate up to at least 9 days after growth was arrested. Analysis of differential transcriptomics and proteomics data collected during growth arrest showed an enrichment of genes or pathways that use ATP. Based on this, we suggest that *Synechocystis* that are growth arrested by citrate synthase repression are unable to metabolize ATP and NADPH in the proper ratios (Erdrich et al., 2014; Shabestary and Hudson, 2016). As a way to prevent irreversible growth arrest and decline of metabolic activity, we propose and test intermittent growth arrest of lactate-secreting *Synechocystis* as a way to increase the average metabolic activity during two-stage production. This strategy significantly increased cumulative lactate titers, and allowed stable lactate production in bench-scale bioreactors for one month.

2. Results

2.1. Growth arrest of Synechocystis increases titers but reduces metabolic activity over time

We have previously shown that CRISPRi of the essential enzyme citrate synthase *(Acetyl-CoA + Oxaloacetate → Citrate; sll0401)* in *Synechocystis* blocks carbon flux from entering the TCA cycle. The primary effect of GltA repression is a growth arrest, as cells cannot synthesize 2-oxoglutarate, the precursor for the amino acid glutamate. The flux alteration can be exploited to increase the productivity of heterologous products derived from acetyl-CoA or pyruvate, such as n-butanol (Shabestary et al., 2018) and L-lactate (Yao et al., 2020) (Fig. 1A).

We first characterized CRISPRi-induced growth arrest in lactate-secreting *Synechocystis* strains. We chose L-lactate as a product of choice since it is close to central metabolism, and can ensure a sufficient carbon sink upon biomass repression (Oliver and Atsumi, 2014). The *Synechocystis* strain encoded a mutant lactate dehydrogenase (Ldh) with increased NADPH/NADH selectivity, derived from *Lactococcus lactis* (Angermayr et al., 2014). An Ldh that uses both NADPH and NADH takes advantage of the large NADPH pool that is connected to the light reactions, a pool that may increase upon repression of biomass formation. Strain KS177 contained Ldh, dCas9 and two sgRNAs targeting *gltA*. Both dCas9 and sgRNAs were cloned under the P_{L22} promoter, which is tightly repressed, but can be induced with added anhydrotetracycline (aTc). Strain KS171 served as a control as it contained the Ldh and dCas9 but no sgRNAs. Both KS171 and KS177 were cultivated in batch, and CRISPRi was induced in both cultures by addition of aTc.

While CRISPRi induction is presumed to halt *gltA* transcription and GltA protein synthesis quickly, the GltA protein pool must be depleted before a growth-arrest phenotype is observed. The growth curve of KS177 diverged from the control strain KS171 at 24 h, and full growth arrest occurred at 48 h, approximately four cell generations (Fig. 1B). The subsequent growth-arrest (GA) phase for KS177 showed improved lactate titers compared to the non-GA strain KS171, and carbon partitioning to lactate exceeded 90% (Fig. 1C and D). To remove the potential contribution of a higher perceived light on increased productivity in the growth-arrested KS177, we also cultivated both strains in turbidostat, where OD_{730} was held constant. The KS177 strain again had significantly higher lactate titers 24 h after addition of aTc (Fig. S1). Therefore, in addition to allowing better light penetration, the growth arrest also rerouted assimilated carbon towards product synthesis.

The specific CO_2 uptake rate of KS171 and KS177 reached 2.5 mmol CO_2/gDCW/hr at 48 h for both KS177 and KS171 and then declined to 0.3 mmol CO_2/gDCW/hr (KS171) and 0.7 mmol CO_2/gDCW/hr (KS177) at 140 h. Though we estimated the CO_2 uptake rate using CO_2 sensor measurements of gas composition in the inlet and outlet feeds, which is not as accurate as isotope tracing, the calculated maximum specific CO_2 uptake rate of KS171 and KS177 is similar to the 3.7 mmol CO_2/gDCW/hr maximum uptake rate of wild type *Synechocystis* measured using ^{13}C-labled CO_2 (Young et al., 2011).

The reduced specific CO_2 uptake rate in KS171 can be attributed to increased light-shading and entrance into stationary phase. For the growth arrested KS177, CO_2 uptake was reduced even though light, CO_2, and other nutrients were abundant. The absorbance spectrum of the growth-arrested KS177 suggested stressful conditions already 24 h after addition of aTc and when the growth rate was not yet affected, as KS177 had a decrease in phycocyanin and chlorophyll A compared to KS171 at 24 h and 96 h post induction (Fig. S2). The reduction in chlorophyll A in KS177 during growth arrest was confirmed in a separate experiment by

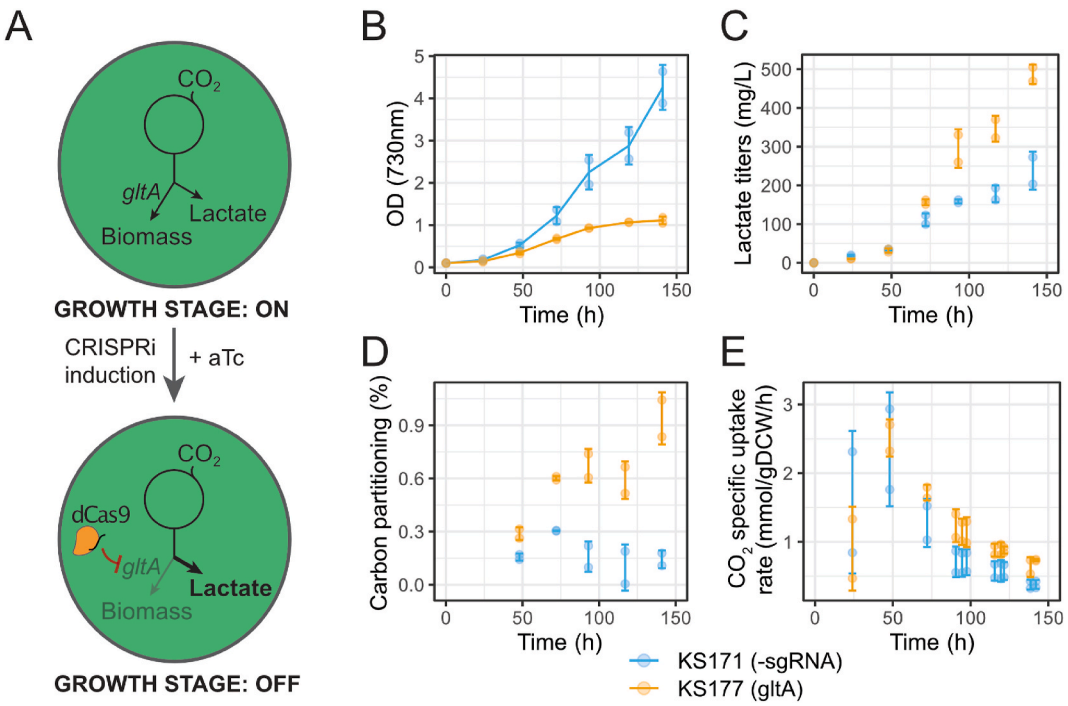

Fig. 1. Overview of CRISPRi mediated growth-arrest (GA) of *Synechocystis*. (A) Induction of CRISPRi by aTc represses *gltA*, which reroutes carbon flux away from the TCA cycle and glutamate synthesis and instead to lactate. **(B)** Growth curves of the GA strain (KS177) and a non-GA control strain (KS171) after aTc addition at time 0. **(C)** Titer of L-lactate in media from cultures in B. **(D)** Carbon partitioning to L-lactate, calculated from specific L-lactate productivity and growth rates. **(E)** CO_2 specific uptake rates calculated from gas flow rate and CO_2 content of exit gas. Cultivations were done in duplicate in a Multi-Cultivator in batch mode, at 30 °C and with white light intensity 300 μmol photons/m^2/s. Starting cell density for all cultures was OD_{730} = 0.1. *gltA:* citrate synthase; *aTc:* anhydrotetracycline. Error bars are standard errors from two parallel cultivations.

chlorophyll A extraction to be 50% (Fig. S4).

The decrease in pigmentation can indicate phycobilisome degradation and chlorosis (Richaud et al., 2001), and can be expected as glutamate is a key precursor in chlorophyll biosynthesis (Vavilin and Vermaas, 2002). These results show that CO_2 uptake during growth arrest is reduced to less than 30% of that of exponential growth.

2.2. Growth arrest by GltA repression can be reversed

One downstream metabolic product of citrate synthase is 2-oxoglutarate, which is central to nitrogen assimilation in *Synechocystis,* both as a reporter of nitrogen status, and in the synthesis of glutamate. The two primary nitrogen assimilation pathways in cyanobacteria are glutamate dehydrogenase (*gdhA*, *slr0710*), which adds ammonium to 2-oxoglutarate to produce glutamate, and glutamine synthetase (encoded by *glnA* and *glnN*), which adds ammonium to glutamate to produce glutamine (Chávez et al., 1999; Muro-Pastor et al., 2005). Depletion of 2-oxoglutarate by repression of citrate synthase could thus alter perceived nitrogen status in *Synechocystis,* leading to a cascade of events that results in growth arrest. However, a reduced 2-oxoglutarate *per se* is not a likely cause of growth arrest, as nitrogen limitation results in an increase in 2-oxoglutarate, and cells experience a reduction in 2-oxoglutarate without problem when shifted from nitrate to ammonium-containing media (Muro-Pastor et al., 2001). Alternatively, depletion of glutamate and glutamine could trigger ribosome stalling and thus cessation of growth, similar to a bacteriostatic translation-inhibiting antibiotic.

In a first attempt to mitigate the effects of citrate synthase repression, we investigated whether supplied glutamate or arginine could rescue growth-arrested cells. Addition of L-glutamate or L-aspartate to 5 mM before *gltA* repression partially prevented growth arrest and increased chlorophyll content, but addition of arginine did not prevent growth arrest (Figs. S3–S5). Addition of L-glutamate to cells that had been in growth arrest for 6 and 9 days also resulted in recovery of growth (Fig. S6). The inability of exogenous glutamate to fully rescue growth could be due to limited uptake by *Synechocystis.* The reported uptake rate of glutamate by *Synechocystis* (300 nmol/min/mg Chl, approximately 0.4 mmol/gDCW/hr (Quintero et al., 2001)) is lower than the estimated flux to glutamate during exponential growth (10 mmol/gDCW/hr (Gopalakrishnan et al., 2018)), though this uptake value was measured at relatively low supplied L-glutamate concentrations (10 mM). Arginine is taken up at higher rates (approximately 2 mmol/gDCW/hr (Labarre et al., 1987)), and can be catabolized to both glutamate and glutamine, although the fraction of arginine converted to glutamate was measured to be less than 5% (Quintero et al., 2000).

We next tested whether extracellular addition of 2-oxoglutarate itself could revert or prevent growth arrest. To facilitate 2-oxoglutarate uptake by *Synechocystis*, we inserted the gene *kgtP* from *E. coli,* encoding a carboxylic acid transporter, into KS177 to create KS201. This transporter was shown to be required for uptake of 2-oxoglutarate by *Synechococcus elongatus* (Quintero et al., 2000; Vázquez-Bermúdez et al., 2000). However, addition of 2-oxoglutarate at 1 mM to KS201 completely inhibited growth, even before *gltA* repression (Fig. S5). An increased 2-oxoglutarate concentration may alter the driving force of lysine biosynthesis, leading to cessation of growth (Asplund-Samuelsson et al., 2018). Due to cell sensitivity, 2-oxoglutarate could not reliably be tested as a rescue metabolite.

Finally, we tested whether removal of the CRISPRi inducer aTc would allow cells to resume growth. We grew the KS177 strain in batch culture, and induced growth arrest by addition of aTc. We withdrew aliquots from this flask at 8 h and 72 h post-induction, washed the cells, and re-suspended them in fresh media without aTc. Both aliquots were able to resume growth in the absence of aTc (Fig. S6).

2.3. ATP and NADPH imbalances occur during growth arrest

To elucidate mechanisms for reduced metabolic activity during GA,

we performed RNASeq on KS177 as it entered the growth arrest phase. KS177 was grown in triplicate turbidostat cultivations and CRISPRi induced with aTc addition. To ensure cells were not photoinhibited at the OD_{720} = 0.4 set-point, we set light intensity at 200 μmol photons/m^2/s. Samples were taken pre-induction (0 h) and at 24 h and 96 h post-induction. These timepoints are long compared to studies on the response to nutrient shift, where typically a 2 h or 4 h time point is sampled (Wang et al., 2004; Krasikov et al., 2012; Orf et al., 2016). However, a 24 h period is approximately one cell doubling, which we estimated would be needed to insure an appreciable depletion of the GltA protein after its transcriptional repression. The 96 h timepoint was chosen because at this time cells were typically growth arrested. After filtering with Principal Component Analysis, triplicates from each time point were further considered for analysis. At 24 h and 96 h post-induction of CRISPRi, growth rate was reduced by 10% and 70%, respectively (Fig. 2A). Gene expression fold-changes (FC) were calculated to compare post-induction and pre-induction expression levels (24 h vs 0 h, and 96 h vs 0 h).

The KS177 transcriptome 24 h after induction of CRISPRi revealed modulation of many genes involved in nutrient transport and homeostasis (Fig. 2B, Table 1, Supplemental Data 1: DESeq2 output). Genes involved in nickel (*nrsBACD* operon) and cobalt (*coaT*, *slr0797*) uptake were significantly down-regulated, while those for nitrate/nitrite uptake (*nrt* genes) and sulfate/thiosulfate uptake (*cys* genes) were significantly up-regulated. The sulfate binding protein *sbpA* transcript had the highest upregulation after 24 h (31-fold). The strong upregulation of sulfur-related genes suggests that cells experience sulfur limitation stress (Richaud et al., 2001; Zhang et al., 2008). However, such a response may also be triggered by a reduction in glutathione, a non-ribosomal peptide synthesized from glutamate and cysteine. Glutathione is not essential for growth in *Synechocystis,* but is essential to tolerate redox perturbations and appears to be important for extended viability in the stationary phase (Cameron and Pakrasi, 2010). Other stress-response genes were also up-regulated, such as those encoding heat-shock proteins, chaperones and chaperonins (*groES*, *slr2075*; *groEL*, *slr2076*; *groEL-2*, *sll0416*; *dnaK2*, *sll0170*; *htpG, sll0430; clpB*, *slr1641*). The *pilA5-pilA6* (*slr1928-slr1929*) operon was also significantly up-regulated.

The transcriptome response at 96 h after induction showed more pronounced changes than at 24 h (Fig. 2C). While the 24 h response has a higher number of statistically significant up-regulations (85 genes) than down-regulations (18 genes), the response after 96 h was enriched in down-regulations, with 466 down-regulations and 344 up-regulations. Among the most significantly downregulated genes were those related to light-harvesting, bioenergetics, and translation, including *cpc* and *apc* genes, encoding various subunits of the phycobilisome, *pet* genes encoding photosynthetic electron transport proteins, *atp* genes coding for subunits of ATP synthetase, and *rpl12* and *rps2,* coding for ribosomal subunits. Again, the most upregulated genes were related to physiological stress. For example, upregulation of pili is common under many stress conditions (Hernández-Prieto et al., 2016). The alternative sigma factor SigF (*rpoF, slr1564*) was slightly but significantly up-regulated at 96 h and is involved in pili formation and is important in salt stress acclimation (Bhaya et al., 1999; Huckauf et al., 2000). The genes *sll1862* and *sll1863* have no annotated function but were also found to be up-regulated during various stresses (Marin et al., 2004; Mironov et al., 2019).

The RNASeq results indicate a moderate stress response already after 24 h, consistent with the reduced levels of chlorophyll and other pigments (Fig. S2), which leads to a severe reduction in metabolic activity at 96 h. Early up-regulation of *nrt* genes indicates a possible nitrogen starvation leading to reduced metabolic activity. However, it is typically the overabundance of 2-oxoglutarate that indicates a lack of nitrogen and triggers the transcriptional cascade of the global nitrogen regulator *ntcA*, activator of *nrt* genes (Fokina et al., 2010; Schwarz and Forchhammer, 2005). A perceived nitrogen limitation during GA is not supported by other genes known to be differentially expressed when

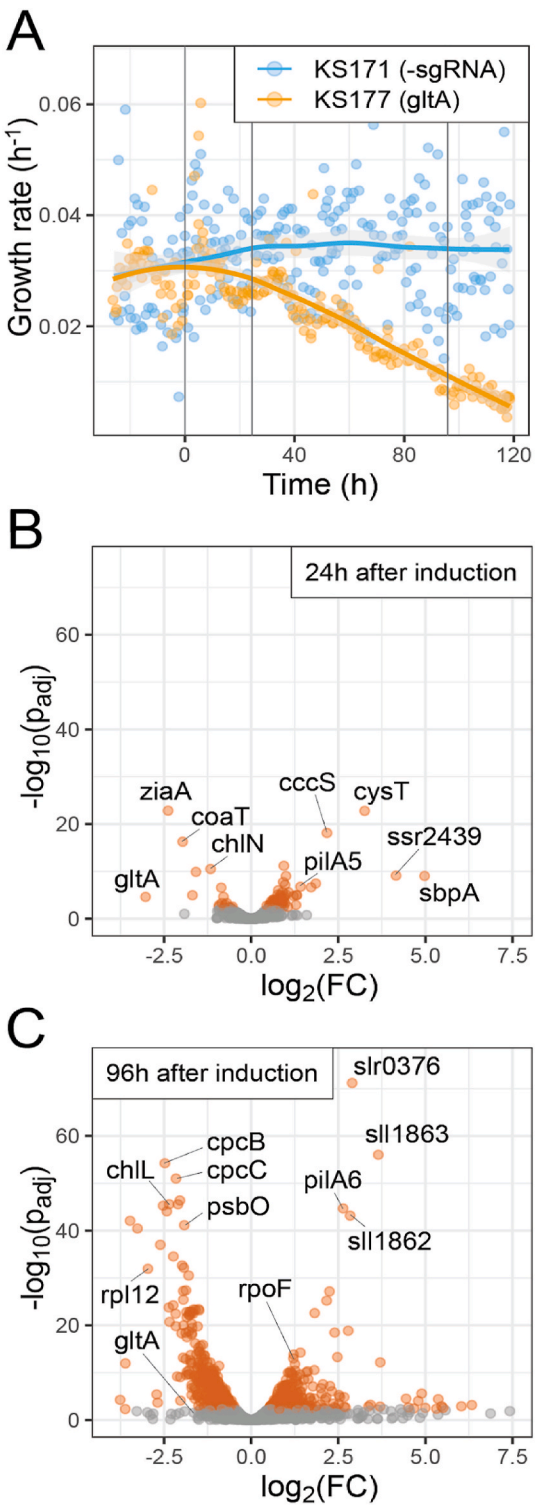

Fig. 2. Transcriptomics of KS177 during growth-arrest by CRISPRi. KS177 was grown in triplicate cultivations in turbidostat mode (OD_{730} = 0.4, white light = 200 μmol photons/m^2/s). Time 0 h marks induction of the CRISPRi of *gltA*. (A) Growth rates of two cultures before and after induction. The lines represent the sampling times for RNAseq. (B) Volcano plot showing differential gene expression in KS177 between pre-induction of CRISPRi and 24 h after induction. (C) Volcano plot showing differential gene expression in KS177 between pre-induction of CRISPRi and 96 h after induction (log2 fold-change). In orange, significantly expressed genes ($P_{adj} < 0.005$). In the volcano plot, points represent averages over three replicates as calculated by DESeq2. (For interpretation of the references to color in this figure legend, the reader is referred to the Web version of this article.)

Table 1
Top 10 up- and down-regulated genes in KS177 measured by RNA-Seq 24 h after induction of CRISPRi.

locus	gene	function	Log Fold Change	p-adjusted
Up-regulated				
slr1453	*cysT*	sulfate/thiosulfate ABC transporter	3.26	1.61E-23
slr1667	*cccS*	related to pilin formation	2.18	7.50E-19
sll0947	*lrtA*	ribosome-associated protein	0.94	6.45E-12
ssr2439	*ssr2439*	hypothetical protein	4.16	7.69E-10
slr1452	*sbpA*	sulfate binding protein	4.97	9.25E-10
sll0253	*sll0253*	hypothetical protein	1.00	9.55E-10
slr0301	*ppsA*	phosphoenolpyruvate synthase	0.92	1.80E-08
slr1454	*cysW*	sulfate transport system permease	1.86	3.58E-08
slr1034	*ycf41*	hypothetical protein	0.97	6.74E-08
slr1928	*pilA5*	type 4 pilin-like protein	1.42	1.71E-07
Down-regulated				
slr0798	*ziaA*	zinc-transport P-type ATPase	−2.38	1.46E-23
slr0797	*coaT*	cobalt-transport P-type ATPase	−1.97	5.31E-17
slr0750	*chlN*	protochlorophyllide reductase subunit N	−1.17	3.06E-11
slr0794	*nrsA*	cation efflux system protein	−1.59	1.24E-10
slr0376	*slr0376*	hypothetical protein	−0.86	2.65E-07
sll0792	*smtB/ziaR*	zinc-responsive transcriptional repressor	−1.68	1.07E-05
slr1634	*slr1634*	hypothetical protein	−0.80	2.23E-05
sll0401	*gltA*	citrate synthase	−3.03	2.44E-05
sll1219	*sll1219*	hypothetical protein	−0.70	0.00047
slr8036	*slr8036*	probable acetyltransferase	−0.84	0.00047

nitrogen is removed, such as *ntcA*, PHB synthesis (*phaAB* and *phaEC* operons), glycogen metabolism (*glgP2*, *glgA1*), which were not significantly altered at the mRNA level. A comparison with a published microarray dataset for *Synechocystis* during N-starvation (Krasikov et al., 2012), revealed only weak correlation (Fig. 3 and Fig. S7). Nitrogen responsive and phycobilisome genes were moderately correlated between the GA transcriptome (24h after induction) and a N-starved transcriptome sampled 24 h after starvation (ranked Spearman correlation 0.27 and −0.19, respectively), but ribosomal genes were negatively correlated between the two conditions (ranked Spearman correlation −0.82). In fact, many ribosomal genes were slightly upregulated at 24 h after induction of CRISPRi, with a median $\log_2$FC = 0.43 for 43 *rps* and *rpl* genes (Supplementary Data 1, Fig. S8). Some ribosome genes were upregulated significantly, such as *rps15* ($\log_2$(FC) = 1.21) and *rpl23* ($\log_2$(FC) = 0.83). We note that comparison of the KS177 strain to nitrogen starvation of a wild type *Synechocystis* could be confounded by a cellular response to lactate synthesis itself, which is increased in KS177 during growth arrest. While the transcriptomics response to lactate synthesis has not been reported, Borirak et al. measured the proteome of a lactate-producing *Synechocystis* and found over 100 differentially expressed proteins compared to a wild type strain. Multiple genes encoding light harvesting proteins, photosystem proteins, and central carbon metabolism enzymes were downregulated in the lactate-producing strain (Borirak et al., 2015). Some of these, such as downregulation of light harvesting, were also observed in KS177 growth arrest response. However, none of the top differentially expressed genes in KS177 were among those reported by Borirak et al.

Faced with a transcriptome that did not appear to mimic a particular stress response, we performed a GO term enrichment on genes that were significantly ($P_{adj} < 0.005$) up-regulated, down-regulated and differentially expressed (both directions) after 24 h. Taking genes that were only down-regulated did not return significant enrichment. However, analysis of up-regulated transcripts revealed enrichment of processes related to response to heat, response to temperature stimulus and protein folding consistent with the initiation of a smooth stress response after 24 h (Table S1; false-discovery rate, FDR < 0.05). For genes that were significantly expressed in both directions, we found genes linked to transmembrane transporter activity, ATP binding and ATPase-coupled

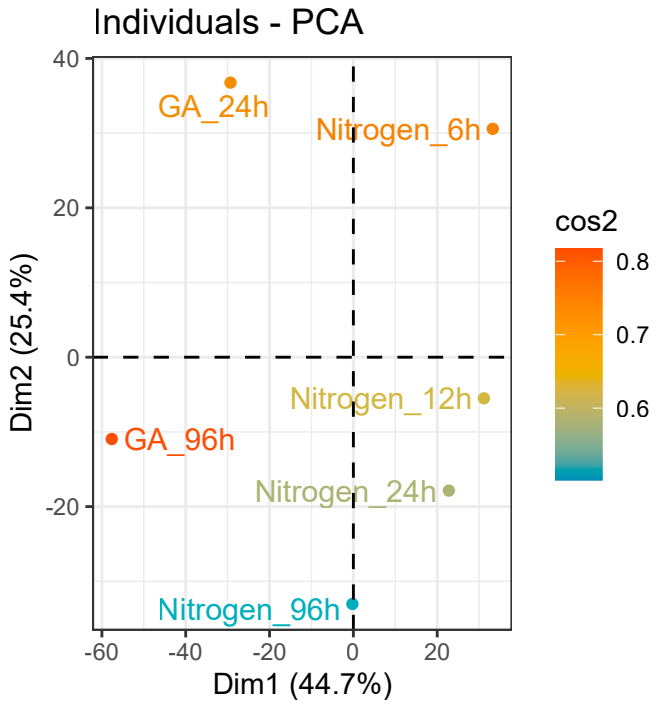

Fig. 3. Principal component analysis of the growth-arrest response of KS177 reported here (GA_24h and GA_96h) and the nitrogen starvation response of *Synechocystis* wild type reported in (Krasikov et al., 2012). The cos2 score indicates the quality of representation by the principal components.

Table 2
GO term enrichment for genes significantly expressed (up- and down-regulations; $P_{adj} < 0.05$) at the transcriptome level in KS177 at 24 h after induction of CRISPRi.

GO biological process complete	fold enrichment	raw p-value	adjusted p-value
ATPase-coupled inorganic anion transmembrane transporter activity (GO:0043225)	15.76	3.15E-04	4.95E-02
sulfur compound transmembrane transporter activity (GO:1901682)	14.18	4.32E-04	4.36E-02
unfolded protein binding (GO:0051082)	11.82	1.57E-04	5.54E-02
ATPase-coupled ion transmembrane transporter activity (GO:0042625)	8.86	1.27E-04	1.80E-01
inorganic anion transmembrane transporter activity (GO:0015103)	7.33	3.12E-04	5.50E-02
anion transmembrane transporter activity (GO:0008509)	5.39	5.17E-04	4.87E-02
ion transmembrane transporter activity (GO:0015075)	3.64	3.16E-04	4.46E-02
ATP binding (GO:0005524)	2.44	3.24E-04	4.16E-02
adenyl ribonucleotide binding (GO:0032559)	2.44	3.30E-04	3.88E-02
adenyl nucleotide binding (GO:0030554)	2.43	3.36E-04	3.65E-02
purine ribonucleoside triphosphate binding (GO:0035639)	2.41	1.50E-04	1.06E-01
purine ribonucleotide binding (GO:0032555)	2.41	1.54E-04	7.23E-02
purine nucleotide binding (GO:0017076)	2.4	1.57E-04	4.45E-02
ribonucleotide binding (GO:0032553)	2.31	2.31E-04	5.43E-02
carbohydrate derivative binding (GO:0097367)	2.28	2.63E-04	5.32E-02

transmembrane transporter activity processes (Table 2). The strong enrichment of processes involving ATP in the affected genes suggests that ATP homeostasis is significantly affected soon after CRISPRi of *gltA*.

2.4. Proteome analysis suggests a role for ATP hydrolysis during growth arrest

While analysis of the transcriptome levels could reveal regulations after GA induction, we aimed to investigate whether those transcript changes were manifested in protein levels and not lost to post-transcriptional buffering (Karlsen et al., 2021). We collected shotgun proteomics data from KS177 before (0 h) and after (48 h) GA induction in a turbidostat mode (OD_{720} = 0.4, light = 200 μmol photons/m^2/s; Supplemental Data 2: Significantly expressed peptides). Proteomics data are more difficult to obtain compared to transcriptomics, due to the diversity in protein physicochemical properties and variable location within the cell. Proteins are denatured and proteolytically digested, resulting in peptide fragments that are then analyzed by LC-MS. Peptides can be assigned unambiguously to each gene (one or more peptides per gene). Here, we report peptides that are significantly altered 48 h after induction in comparison to pre-induction levels (0 h). In total, 120 peptides were significantly altered ($p_{adj} < 0.01$), corresponding to 58 up-regulated and 6 down-regulated proteins. GltA was reduced to 20% at 48 h after induction ($\log_2$(FC) = −2.25). The dCas9 protein was up-regulated, with a $\log_2$(FC) between 3 and 5).

Consistent with the 24 h transcriptomics response, phosphoenolpyruvate synthase (PpsA, *slr0301*) was up-regulated at the protein level after 48 h ($\log_2$(FC) = 1.42), indicating a possible competing reaction for the pyruvate pool (Fig. 4). The small heat shock protein Hsp17 was also significantly up-regulated ($\log_2$(FC) = 1.04) as well as the chaperonin GroEL (*slr2076*, two peptides with $\log_2$(FC) = 1.48 and 2.50). Glycogen metabolism was significantly modulated at the protein level, with up-regulations of GlgC (*slr1176,* $\log_2$(FC) = 1.78) and GlgP (*sll1356,* $\log_2$(FC) = 1.07), involved in glycogen formation and degradation, respectively (Doello et al., 2018). Up-regulation of these two metabolic enzymes together could constitute another ATP wasting mechanism, with a net stoichiometry of one ATP consumed per ADP-glucose (Fig. 4). The increase in glycogen content during growth arrest was confirmed by extraction of and assay of glycogen. Glycogen content in KS177 increased several fold over 6-days following CRISPRi induction, to approximately 50% of the level in N-starved cells (Fig. S9). Surprisingly, several ribosomal proteins were also significantly up-regulated at the protein level, such as Rps18 (*ssr1399*, two peptides with $\log_2$(FC) = 1.54 and 3.44), Rpl1 (*sll1744*, $\log_2$(FC) = 1.07), Rps1a (*slr1356*, $\log_2$(FC) = 2.86) and RpmB (*ssr1604*, $\log_2$(FC) = 1.67). An increase in ribosome proteins is consistent with the slight increase in ribosomal transcripts after 24 h post induction (median $\log_2$(FC) = 0.4 for 43 *rps* and *rpl* genes) as measured from RNA-Seq data (Supplementary Data 1), though at 96 h growth arrest nearly all *rps* and *rpl* transcripts were redcuced (median $\log_2$(FC) = −1.3). Ribosomal protein levels in *Synechocystis* have been shown to correlate with growth rate in the exponential phase (Jahn et al., 2018; Zavřel et al., 2019). An upregulation of ribosomal proteins at a reduced growth rate presents an unusual decoupling.

Given the phototrophic lifestyle of *Synechocystis*, ATP and NADPH buffering mechanisms are vital as cells must adapt to highly variable light intensities. The ATP/NADPH ratio is typically maintained in cyanobacteria through alternative and cyclic electron flows that direct photosynthesis electrons for NADPH, H_2O, or ATP formation. However, energy buffering mechanisms are not always effective in extreme conditions. For example, it was shown that an external supplied electron sink, an aldehyde that could be reduced with NADPH, improved photosynthesis of *Synechocystis* grown in low-C_i conditions, where NADPH presumably accumulates to high levels (Zhou et al., 2016). Though we did not observe alternative electron flow proteins upregulated during growth arrest at the transcript or protein level, we wondered if electron dissipation could be compromised in growth-arrested cells. We measured NADPH in a non-lactate producing strain (KS169) as it entered growth arrest and found that NADPH did accumulate up to 2-fold compared to growing cells (Fig. S10). NADPH accumulation was not observed in the lactate-synthesizing KS177 during growth arrest, likely to the presence of Ldh. We also tested whether an additional electron sink could delay the onset of growth arrest or extend the time before a decrease in metabolic activity. We inserted the gene encoding the cytochrome P450 enzyme CYP1A1 from *Mus musculus* into KS177 to create KS214. CYP1A1 derives electrons directly from the PETC in cyanobacteria (Berepiki et al., 2016). Addition of CYP1A1 abolished lactate formation, suggesting that it is a strong electron sink. The addition of CYP1A1 did not slow the onset of growth arrest, but the strain did retain a higher CO_2 fixation rate than KS177 after induction of CRISPRi (Fig. S11). Together, these results suggest that a buildup of NADPH may contribute to the reduction of CO_2 fixation during growth arrest, but that its accumulation is not the sole factor in cessation of growth.

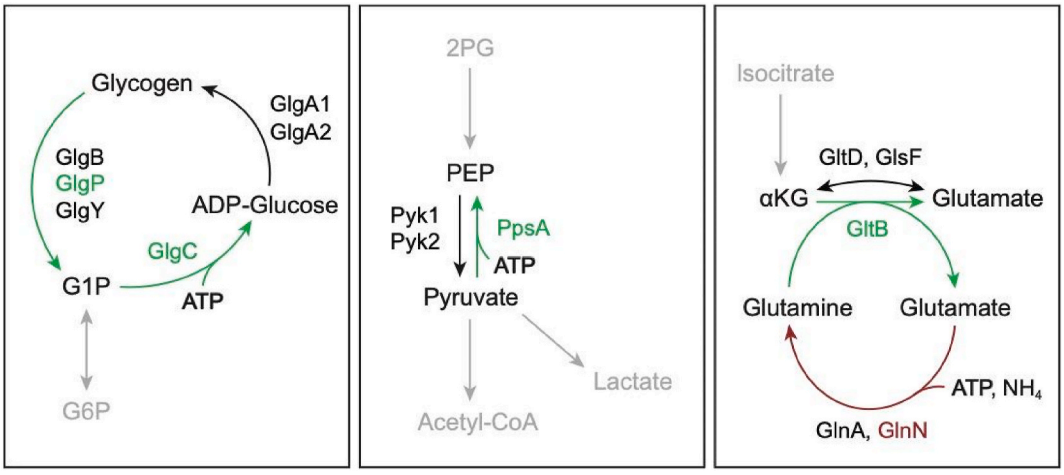

Fig. 4. Potential ATP buffering mechanisms at early stages of growth arrest, based on significantly altered mRNA and protein levels during growth arrest. In green, significantly up-regulated ($p_{adj} < 0.01$) proteins. In red, significantly down-regulated proteins. In grey, surrounding metabolic reactions. Accumulation of glycogen during growth arrest was confirmed by glycogen assay. (For interpretation of the references to color in this figure legend, the reader is referred to the Web version of this article.)

2.5. Alternation between growth and production phases increases overall lactate productivity

The early response to growth arrest (24 h post CRISPRi induction) describes cells that have significant partitioning to lactate, slightly reduced CO_2 uptake rates, and only moderate stress response. However, at 96 h post CRISPRi induction, the stress response is severe, and metabolic activity is reduced significantly. We hypothesized that alternation between growth arrest and normal growth would allow cells to enter a phase with high partitioning to lactate, and subsequently recover from the resulting stress. Such a production system would exploit the reversible nature of CRISPRi-induced growth arrest. A continuous cultivation system would allow the inducer molecule aTc to be gradually washed out of the reactor. While aTc is also degraded in the light, with a half-life estimated at 48 h at the light intensities used here (Behle et al., 2020), as shown below, cells could be growth arrested for at least 15 d without additional aTc.

We set up cultivations of KS177 for growth in turbidostat and designed three inducer-addition regimes (Fig. 5A). A control regime consisted of no added aTc; these cells would not have *gltA* repressed and not enter growth arrest. Regime 1 entailed adding aTc only when cells were at maximum growth, *i.e.* once at the beginning of the cultivation, and again when cells had recovered from growth arrest phase. Regime 2 entailed extra addition of aTc once cells had reached growth-arrest. Here, aTc would not be washed out, as cells were not growing. Regime 2 thus mimics a constant growth arrest in batch culture. For each regime, we monitored growth rate and lactate productivity.

In the control regime (no added aTc), growth rate and lactate productivity were steady for approximately 20 d, after which there was a loss of lactate productivity and a concomitant increase in growth rate in both replicate cultures (Fig. 5A and Fig. S12). In the two test regimes, the first addition of aTc induced CRISPRi and reduced growth rate to nearly zero after 10 d. At this point, a second bolus of aTc was added to Regime 2 cultivations. Regime 1 cultivations recovered from growth-arrest over 2 d, as aTc was washed out. Regime 1 could be switched between growth and production three times over 30 d, after which cells could no longer be growth arrested with additional aTc, likely due to revertants that had mutated dCas9 or sgRNAs. Regime 2 cultivations were growth arrested for 15 d after the last aTc addition (Fig. 5B). This extended growth arrest could be due to higher amounts of aTc which, though not toxic in itself, could keep GltA repressed longer.

Cumulative lactate titers from all cultures were estimated from lactate concentrations measured in culture supernatants and recorded dilution rates from the turbidostats (Supplementary Note 2 for calculation). The control cultivation lost lactate production after 20 d, despite a lower carbon partitioning to product than the growth-arrested cultivations. The periodic growth-arrested cultures (Regime 1) lost lactate productivity at 30 d (Fig. 5C). The consistent loss of lactate productivity is due to lactate-negative revertants that spontaneously arise early in the cultivation, and, due to their faster growth rate, overtake cultures (Du et al., 2017). In the oscillating growth-arrest cultivations, the oscillations in lactate partitioning were counterphase to growth rate and total

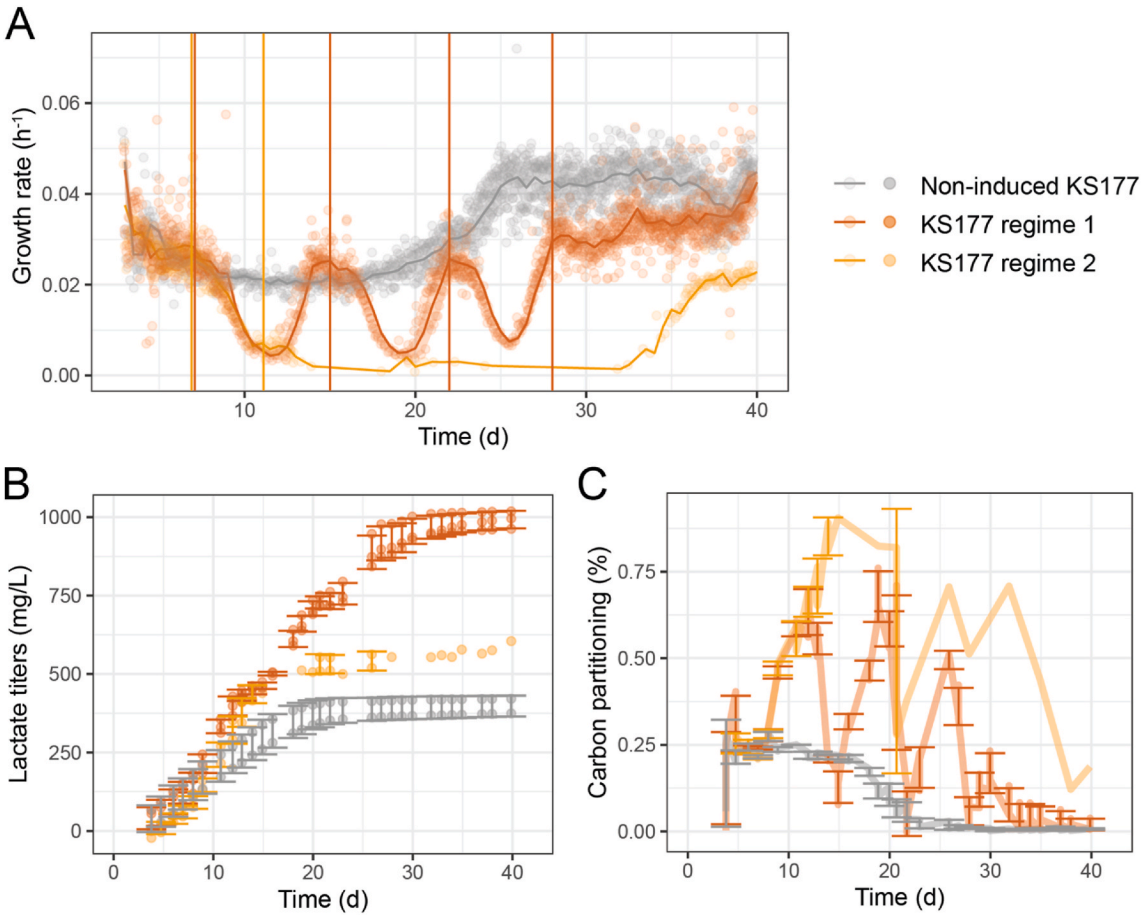

Fig. 5. Intermittent growth arrest in KS177 and its effect on lactate production. (A) Growth rates. Vertical lines represent addition of aTc (0.5 μg/mL). For regime 1, aTc was added at the peak of each growth-rate oscillation. For regime 2, additional addition of aTc prevented cells from returning from GA. (B) Cumulative lactate titers over time. Calculations were based on lactate concentrations in reactors and turbidostat dilutions (Supplementary Note 2). (C) Partitioning of fixed carbon to lactate. Cells were cultivated in a turbidostat mode at 30 °C with setpoint OD_{720} = 1 and a light regime 330 μmol photons/m^2/s per OD_{720} unit. Regime 1 was performed in triplicate cultivations. Regime 2 and the control regime were performed in duplicate cultivations.

cumulative titers reached 1 g/L after 30 d. An increase 2.5-fold higher than the control cultivation.

3. Discussion

We characterized the growth arrest of *Synechocystis* following CRISPRi-based repression of *gltA*. Targeting citrate synthase had a clear positive impact on the specific productivity of lactate, but long-term growth arrest led to a decrease in metabolic activity as CO_2 uptake and lactate productivity were reduced approximately 3 d after induction of CRISPRi. Analysis of the early transcriptome and proteome response (24 h after CRISPRi induction) revealed a stress response that could indicate reduced glutathione and altered ATP homeostasis. As a result, a mixture of stress responses are initiated. Ribosomal proteins remained high, resulting in a conflict with the cellular dormancy that usually accompanies stress conditions.

We hypothesize that an increase in ATP levels during growth arrest results in an alteration of ATP homeostasis. The proteome response at 48 h showed induction of several futile cycles that would hydrolyze ATP, such as glycogen formation/degradation and up-regulation of Ppsa. Previous reports have shown that glycogen synthesis is an important ATP buffering mechanism in *Synechocystis* (Cano et al., 2018). Both the PpsA/Pyk futile cycle and forced ATP hydrolysis by overexpression of ATP-hydrolyzing subunits were recently purposefully implemented in *E. coli* as a way to waste ATP and increase lactate production during nitrogen starvation (Boecker et al., 2019; Hädicke et al., 2015). Moreover, growth-arrested *Synechcoystis* showed an increase in some ribosomal proteins, which was also reported in *E. coli* during CRISPRi of an essential enzyme in nucleotide biosynthesis (Landberg et al., 2020). An upregulation of ribosome protein seems contradictory to the observed reduced growth rate. However, it has been shown that an increase in ATP levels induces transcription of rRNA operons in *E. coli* (Schneider et al., 2002), and that reduced ATP levels (by forced ATP hydrolysis) in *E. coli* led to a downregulation of ribosomes (Holm et al., 2010). An increased ATP levels as cells enter a growth-arrested state could thus lead to increased expression of ribosomal proteins. However, a significant reduction in translation due to limited charged tRNAs could result in further increased ATP levels, so that crucial Mg^{2+} is stripped from the ribosome complex, leading to dissociation and halting of translation. At this time, transcription of ribosomal genes is stopped and transcripts degrade. An accumulation of ATP and resulting decrease in ADP would be expected to reduce metabolic activity by altering reaction driving forces and acidifying the thylakoid lumen.

For bioproduction, forced ATP burning can be beneficial. While the presence of Ldh in GA *Synechocystis* did prevent NADPH accumulation, the ATP/NADPH requirement of this product (<1.5) is lower than that of biomass formation (>2 (Erdrich et al., 2014);). Since forced growth arrest leads to 90% carbon partitioning to lactate synthesis, ATP and NADPH consumption rates are altered. It is possible that ATP is not sufficiently dissipated through lactate synthesis and instead must be hydrolyzed to allow sufficient regeneration of ADP for photosynthesis to continue. Increasing the ATP demand of the production pathway or addition of extra ATP sinks could stabilize metabolic activity during growth-arrest of *Synechocystis*.

As an alternative to forced ATP hydrolysis, we propose here a novel strategy relying on alternation of GA and growth recovery phases. Such oscillations allow protein biosynthesis to rebalance excess ATP and replenish depleted metabolites and proteins. This cultivation regime increased the overall productivity of cultures, leading to more lactate produced for a longer time. While we relied on external addition of an inducer compound, and its light-sensitivity, GltA levels could be coupled to internal oscillators, such as the cyanobacterial circadian clock, where some genes oscillate under constant light depending on the strain (Beck et al., 2014; van Alphen and Hellingwerf, 2015), or synthetic biology oscillators (Elowitz and Leibler, 2000).

4. Methods

4.1. Strains and cultivation conditions

Synechocystis glucose-tolerant wild type strains, obtained from D. Bhaya, University of Stanford, Stanford CA, were transformed via natural transformation and genomic integration using a pMD19-T targeting vector as backbone (Takara). The construct tetR_PL22_dCas9_SpR was integrated at the *psbA1* locus and Ptrc_ldh_CmR was integrated at the *slr0168* locus to make the base strain KS171. The *ldh* gene is from *Lactococcus lactis* with a L39R substitution to display increased specificity towards NADPH (Angermayr et al., 2014). The sgRNA cassette PL22_sgRNAs(gltA_33, gltA_155)_NatR was integrated at the *slr2030-2031* loci to obtain KS177. The sgRNA cassette consists of two sgRNAs targeting *gltA*, binding 33 and 155 bp downstream of the transcription start site. Successful transformants were confirmed with colony PCR and Sanger sequencing. *Synechocystis* strains were cultivated in BG11 medium buffered to pH 7.9 with 25 mM HEPES.

Pre-cultures were grown in shake flasks in a climatic chamber (Percival Climatics) at 30 °C with 40–80 μmol photons/m^2/s white light intensity and 1% CO_2 atmosphere. Cultivations for lactate quantification, RNA-Seq, proteomics, and L-glutamate supplementation were performed in a multi-channel photobioreactor (Multi-Cultivator MC-1000-OD, Photon System Instruments) at 30 °C with 1% CO_2 in air bubbled through the culture reactor (80 mL) and illuminated as indicated in the text. In the case of turbidostat growth, the setpoint for OD_{720} was typically 0.2, except in the case of the periodic repression experiments (Fig. 5), where target OD_{720} = 1.0. The OD_{720} was measured automatically every 5 min by an in-house software package (pycultivator, https://gitlab.com/mmp-uva/pycultivator) which also controlled light intensity and peristaltic pumps (Reglo ICC, ISMATEC, Germany). The specific growth rate was estimated from how quickly OD_{720} increased after a pulse of fresh media. When cell density reached the target OD_{720}, a 5% vol bolus of fresh media was automatically injected and the same volume pumped out of the reactor. The OD_{720} was monitored online following this dilution. A linear regression model was fitted to the natural logarithm of OD_{720} vs time (in hours) for each dilution cycle. The slope of this model was assumed to be the specific growth rate.

Cultures were supplemented with antibiotics (12.5 μg/mL chloramphenicol, 25 μg/mL spectinomycin, 5 μg/mL nourseothricin) and the inducer aTc (1 μg/mL) when appropriate. When cultures were selected with the antibiotic gentamicin (2 μg/mL), sodium thiosulfate was supplemented in liquid media (3 g/L). A list of *Synechocystis* strains used in this study is available as supplementary material (Table S2).

4.2. CO_2 measurement

When grown in the multi-cultivator, CO_2 from the gas outlet was recorded online using a Cozir CM-0124 CO_2 sensor (CO2Meter.com). The CO_2 uptake rate was calculated using the difference between the inlet (measured to be 1% CO_2 by volume) and outlet gas CO_2 content and gas flow rate.

4.3. L-lactate measurement

L-Lactate was measured using a fluorometric assay. For the fluorometric assay, 300 μL of culture from flask or turbidostat was sampled, pelleted at 4000 g for 6 min at 4°C and the supernatant stored at −20°C until analysis. The samples were analyzed with a L-Lactate Assay kit (Cayman Chemical) according to the manufacturer's protocol on a 96 well-plate (Greiner clear) using a spectrophotometer (Spectramax i3x, Molecular Devices).

4.4. Absorption spectrum

Cells were harvested at an amount equal to 2 mL $OD_{730} = 0.2$ and were centrifuged at 4000 g for 6 min. The pellet was resuspended in 400 μL fresh BG11 media and absorption between 300 and 800 nm was recorded (Spectramax i3x, Molecular Devices) in quadruplicates.

4.5. Carbon partitioning

Carbon partitioning was calculated as the carbon flux going to lactate (specific productivity r_P in Cmol/gDCW/h) over the flux going to biomass (growth rate r_X in Cmol/gDCW/h) and lactate (r_P in Cmol/gDCW/h):

$$C_{partioning}[\%] = \frac{r_P}{r_P + r_X}$$

The specific productivity at a given timepoint t_i was calculated as the difference in titers with the previous timepoint t_{i-1} over the difference in time multiplied by the OD at t_i, then converted in C-mol. For biomass carbon content, we assumed a composition of $C_4H_7O_2N$ (Angermayr et al., 2012).

4.6. NADPH quantification

A luminescence kit was used to quantify NADPH (Promega). NADPH was quantified from cultures grown in duplicates in a turbidostat to ensure equal light shading across mutants (OD_{730} at 0.4, light intensity at 200 μE). Cultures (10 mL) were pelleted at 4000g for 10 min at 4 °C. The pellets were resuspended in 200 μL of cold 0.2 M NaOH + 1% (w/vol) DTAB. Glass beads were added (100 μL), samples were vortexed for 30 min at 4 °C and centrifuged at 10000 g for 10 min at 4 °C. The supernatants were analyzed with the NADP/NADPH-Glo Assay Kit (Promega) according to the manufacturer's protocol.

4.7. RNA extraction and sequencing

RNAseq was performed on KS177 strains grown in turibodstat in quadruplicate (OD = 0.4, light = 200 μmol photons/m^2/s), before induction (0 h) as well as 24 h and 96 h after induction. Cells ($OD_{730} = 0.4$, 15 mL) were collected by centrifugation for 10 min at 5000 g at 4 °C and total RNA was extracted using the GeneJet RNA purification kit (ThermoFisher). The manufacturer's instructions were followed except that lysozyme was added to the TE buffer to 40 mg/L instead of 0.4 mg/L. Beads were also used to lyse the cells. DNA was removed using the RapidOut DNA Removal Kit (Thermo Fisher). Ribosomal RNA was depleted from the samples using the Ribominus Bacteria 2.0 Transcriptome Isolation Kit (Thermo Fisher/Invitrogen) according to the manufacturer's protocols. Purified RNA samples were further fragmented, reverse-transcribed and indexed using the NEBNext Ultra Directional RNA Library Prep Kit for Illumina (Product number E7420S, New England BioLabs). The indexed cDNA samples were quantified using the Qubit (Thermo Fisher) and the Bioanalyzer (Agilent). Samples were pooled together (in equimolar ratio) and sequenced on an Illumina NextSeq 500 System using the NextSeq 500/550 High Output v2 kit (75 cycles). Sequencing reads were filtered and mapped to the genome using Ribopipe (https://github.com/Asplund-Samuelsson/ribopipe (Karlsen et al., 2018)). In short, adapters were removed from the reads with cutadapt, bad quality reads were removed with sickle, and bowtie was used to filter out rRNA and tRNA reads and assign the remaining reads to the *Synechocystis* genome (Reference genome NCBI NC_000911.1; https://www.ncbi.nlm.nih.gov/nuccore/NC_000911.1). Principal Component Analysis was used to filter out outliers. After filtering, analysis was performed in triplicate for KS177 strain at 0 h, 24 h and 96 h DESeq2 was used to determine fold changes between conditions (design = time) as well as significance with a multiple hypothesis adjusted p-value, Benjamini-Hochberg procedure (Love et al., 2014). The 0h transcriptome was used as reference to compute log-fold changes (24 h vs 0 h, 96 h vs 0 h).

4.8. Gene-ontology enrichment

Significantly ($p_{adj} < 0.005$) differentially expressed genes (up-regulated, down-regulated or both) were enriched for GO term associations using the online gene ontology resource (http://geneontology.org). Significant genes were extracted (locus name) and converted to their UniProtID identifiers. Molecular function, biological process and cellular component were investigated.

4.9. Protein extraction and LC-MS/MS

A protocol is available as a Supplementary Note. In short, cells pellets ($OD_{730} = 0.4$, 20 mL) were collected by centrifugation for 10 min (5000 g) at 4 °C and stored at −80 °C until further analysis. Cells were mechanically lysed, and proteins were extracted using a Zeba Spin Desalting column (Thermo Scientific) and then quantified through a Bradford assay (BioRad). Total proteins were denatured using DTT in sodium deoxycholate at 96 °C and samples were incubated at room temperature in the dark with iodoacetamide to prevent disulfide bonds from reforming. Denatured proteins were further digested with LysC for 3h and Trypsin for 16 h at 37 °C. Formate was added to stop the digestion and samples were centrifuged at 14000 g for 10 min to remove the supernatant and samples were stored at −20 °C until quantification was performed. Peptide quantification was performed on a Q-exactive HF Hybrid Quadrupole-Orbitrap Mass Spectrometer (Thermo Scientific) coupled with an UltiMate 3000 RSLCnano System (Thermo Scientific; CA, USA) using a C18 Acclaim PepMap 100 trap column (Thermo Scientific; CA,USA; 75 μm x 2 cm, 3 μm, 100Å) and an ES802 EASY-Spray PepMap RSLC C18 Column (Thermo Scientific; CA,USA; 75 μm x 25 cm, 2 μm, 100 Å) for separation. Peptide fragments were assigned to the *Synechocystis* genome (UniProt reference UP000001425 with the addition of the lactate dehydrogenase and dCas9 proteins) using EncyclopeDIA (Searle et al., 2018), against a predicted library generated with Prosit (Gessulat et al., 2019) and statistical analysis was performed group-wise with the MSstats package in R.

4.10. Glycogen measurement

Three separate cultures of KS177 were started in a Multicultivator in turibodstat mode ($OD_{720} = 0.2$, light = 150 μmol photons/m^2/s) in a Multicultivator. Once culture growth stabilized, aTc was added to induce growth arrest (t = 0). Culture samples (15 mL) were taken pre-induction (t = 0), 1 d, 2 d, and 6 d post induction for glycogen assay. The samples were pelleted (6000 g, 5 min), washed once with ddH_2O, pelleted again and the supernatant decanted. Pellets were snap-frozen in LN_2 and stored at −80 °C until assay. The glycogen assay of the pellets involved ethanol precipitation, enzymatic degradation, and colorimetric assay of free sugars, and followed the protocol of (Koch et al., 2019) with minimal differences. The amyloglucosidase was a 30-60 U/mg powder formulation (Sigma-Aldrich A7420) with < 0.02% glucose content. Relative glycogen content was reported as OD_{645}/OD_{720}.

CRediT authorship contribution statement

Kiyan Shabestary: Conceptualization, Investigation, Formal analysis, Data curation, Writing – original draft, Writing – review & editing. **Hugo Pineda Hernández:** Conceptualization, Investigation, Writing – original draft, Writing – review & editing. **Rui Miao:** Conceptualization, Investigation, Writing – review & editing. **Emil Ljungqvist:** Investigation. **Olivia Hallman:** Investigation. **Emil Sporre:** Investigation, Writing – review & editing. **Filipe Branco dos Santos:** Conceptualization, Supervision, Funding acquisition, Writing – review & editing. **Elton P. Hudson:** Conceptualization, Supervision, Funding acquisition,

Project administration, Writing – original draft, Writing – review & editing.

Acknowledgements

We thank Jan Karlsen and Nick Crang at KTH Royal Institute of Technology for help with the Illumina sequencing. We also thank Lim Cheng Kai for fruitful discussions. This work was funded by the European Union's Horizon 2020 research and innovation program under Grant Agreement No. 760994 (ENGICOIN project), The Swedish Research Council (2020-04329) and the Novo Nordisk Fonden (NNF20OC0064371 and NNF20OC0061469).

Appendix A. Supplementary data

Supplementary data to this article can be found online at https://doi.org/10.1016/j.ymben.2021.09.010.

References

Abramson, B.W., Lensmire, J., Lin, Y.-T., Jennings, E., Ducat, D.C., 2018. Redirecting carbon to bioproduction via a growth arrest switch in a sucrose-secreting cyanobacterium. Algal Res 33, 248–255.

Adams, C., Godfrey, V., Wahlen, B., Seefeldt, L., Bugbee, B., 2013. Understanding precision nitrogen stress to optimize the growth and lipid content tradeoff in oleaginous green microalgae. Bioresour. Technol. 131, 188–194.

Ajjawi, I., Verruto, J., Aqui, M., Soriaga, L.B., Coppersmith, J., Kwok, K., Peach, L., Orchard, E., Kalb, R., Xu, W., Carlson, T.J., Francis, K., Konigsfeld, K., Bartalis, J., Schultz, A., Lambert, W., Schwartz, A.S., Brown, R., Moellering, E.R., 2017. Lipid production in Nannochloropsis gaditana is doubled by decreasing expression of a single transcriptional regulator. Nat. Biotechnol. 35, 647–652.

Angermayr, S.A., Paszota, M., Hellingwerf, K.J., 2012. Engineering a cyanobacterial cell factory for production of lactic acid. Appl. Environ. Microbiol. 78, 7098–7106.

Angermayr, S.A., van der Woude, A.D., Correddu, D., Vreugdenhil, A., Verrone, V., Hellingwerf, K.J., 2014. Exploring metabolic engineering design principles for the photosynthetic production of lactic acid by Synechocystis sp. PCC6803. Biotechnol. Biofuels 7, 99.

Asplund-Samuelsson, J., Janasch, M., Hudson, E.P., 2018. Thermodynamic analysis of computed pathways integrated into the metabolic networks of E. coli and Synechocystis reveals contrasting expansion potential. Metab. Eng. 45, 223–236. https://doi.org/10.1016/j.ymben.2017.12.011.

Beck, C., Hertel, S., Rediger, A., Lehmann, R., Wiegard, A., Kölsch, A., Heilmann, B., Georg, J., Hess, W.R., Axmann, I.M., 2014. Daily expression pattern of protein-encoding genes and small noncoding RNAs in synechocystis sp. strain PCC 6803. Appl. Environ. Microbiol. 80, 5195–5206.

Behle, A., Saake, P., Germann, A.T., Dienst, D., Axmann, I.M., 2020. Comparative dose–response analysis of inducible promoters in cyanobacteria. ACS Synth. Biol. 9, 843–855. https://doi.org/10.1021/acssynbio.9b00505.

Berepiki, A., Hitchcock, A., Moore, C.M., Bibby, T.S., 2016. Tapping the unused potential of photosynthesis with a heterologous electron sink. ACS Synth. Biol. 5, 1369–1375.

Bhaya, D., Watanabe, N., Ogawa, T., Grossman, A.R., 1999. The role of an alternative sigma factor in motility and pilus formation in the cyanobacterium Synechocystis sp. strain PCC6803. Proc. Natl. Acad. Sci. U. S. A. 96, 3188–3193.

Boecker, S., Zahoor, A., Schramm, T., Link, H., Klamt, S., 2019. Broadening the scope of enforced ATP wasting as a tool for metabolic engineering in Escherichia coli. Biotechnol. J. 14, e1800438.

Borirak, O., de Koning, L.J., van der Woude, A.D., Hoefsloot, H.C., Dekker, H.L., Roseboom, W., de Koster, C.G., Hellingwerf, K.J., 2015. Quantitative proteomics analysis of an ethanol- and a lactate-producing mutant strain of Synechocystis sp. PCC6803. Biotechnol. Biofuels 8, 111. https://doi.org/10.1186/s13068-015-0294-z.

Brockman, I.M., Prather, K.L.J., 2015. Dynamic metabolic engineering: new strategies for developing responsive cell factories. Biotechnol. J. 10, 1360–1369.

Cameron, J.C., Pakrasi, H.B., 2010. Essential role of glutathione in acclimation to environmental and redox perturbations in the cyanobacterium Synechocystis sp. PCC 6803. Plant Physiol 154, 1672–1685.

Cano, M., Holland, S.C., Artier, J., Burnap, R.L., Ghirardi, M., Morgan, J.A., Yu, J., 2018. Glycogen synthesis and metabolite overflow contribute to energy balancing in cyanobacteria. Cell Rep. 23, 667–672.

Chávez, S., Lucena, J.M., Reyes, J.C., Florencio, F.J., Candau, P., 1999. The presence of glutamate dehydrogenase is a selective advantage for the Cyanobacterium synechocystis sp. strain PCC 6803 under nonexponential growth conditions. J. Bacteriol. 181, 808–813.

Chubukov, V., Sauer, U., 2014. Environmental dependence of stationary-phase metabolism in Bacillus subtilis and Escherichia coli. Appl. Environ. Microbiol. 80, 2901–2909.

Doello, S., Klotz, A., Makowka, A., Gutekunst, K., Forchhammer, K., 2018. A specific glycogen mobilization strategy enables rapid awakening of dormant cyanobacteria from chlorosis. Plant Physiol 177, 594–603.

Dunlop, M.J., Keasling, J.D., Mukhopadhyay, A., 2010. A model for improving microbial biofuel production using a synthetic feedback loop. Syst. Synth. Biol. 4, 95–104.

Durante-Rodríguez, G., de Lorenzo, V., Nikel, P.I., 2018. A post-translational metabolic switch enables complete decoupling of bacterial growth from biopolymer production in engineered Escherichia coli. ACS Synth. Biol. 7, 2686–2697.

Du, W., Angermayr, S.A., Jongbloets, J.A., Molenaar, D., Bachmann, H., Hellingwerf, K.J., Branco Dos Santos, F., 2017. Nonhierarchical flux regulation exposes the fitness burden associated with lactate production in synechocystis sp. PCC6803. ACS Synth. Biol. 6, 395–401.

Du, W., Burbano, P.C., Hellingwerf, K.J., Branco Dos Santos, F., 2018. Challenges in the application of synthetic biology toward synthesis of commodity products by cyanobacteria via "direct conversion. Adv. Exp. Med. Biol. 1080, 3–26.

Elowitz, M.B., Leibler, S., 2000. A synthetic oscillatory network of transcriptional regulators. Nature 403, 335–338.

Erdrich, P., Knoop, H., Steuer, R., Klamt, S., 2014. Cyanobacterial biofuels: new insights and strain design strategies revealed by computational modeling. Microb. Cell Fact. 13, 128.

Farmer, W.R., Liao, J.C., 2000. Improving lycopene production in Escherichia coli by engineering metabolic control. Nat. Biotechnol. 18, 533–537.

Fokina, O., Chellamuthu, V.-R., Forchhammer, K., Zeth, K., 2010. Mechanism of 2-oxo-glutarate signaling by the Synechococcus elongatus PII signal transduction protein. Proc. Natl. Acad. Sci. U. S. A. 107, 19760–19765.

Gadkar, K.G., Doyle Iii, F.J., Edwards, J.S., Mahadevan, R., 2005. Estimating optimal profiles of genetic alterations using constraint-based models. Biotechnol. Bioeng. 89, 243–251.

Gessulat, S., Schmidt, T., Zolg, D.P., Samaras, P., Schnatbaum, K., Zerweck, J., Knaute, T., Rechenberger, J., Delanghe, B., Huhmer, A., Reimer, U., Ehrlich, H.-C., Aiche, S., Kuster, B., Wilhelm, M., 2019. Prosit: proteome-wide prediction of peptide tandem mass spectra by deep learning. Nat. Methods 16, 509–518.

Gopalakrishnan, S., Pakrasi, H.B., Maranas, C.D., 2018. Elucidation of photoautotrophic carbon flux topology in Synechocystis PCC 6803 using genome-scale carbon mapping models. Metab. Eng. 47, 190–199.

Hädicke, O., Bettenbrock, K., Klamt, S., 2015. Enforced ATP futile cycling increases specific productivity and yield of anaerobic lactate production in Escherichia coli. Biotechnol. Bioeng. 112, 2195–2199.

Hernández-Prieto, M.A., Semeniuk, T.A., Giner-Lamia, J., Futschik, M.E., 2016. The transcriptional landscape of the photosynthetic model cyanobacterium synechocystis sp. PCC6803. Sci. Rep. 6, 22168.

Holm, A.K., Blank, L.M., Oldiges, M., Schmid, A., Solem, C., Jensen, P.R., Vemuri, G.N., 2010. Metabolic and transcriptional response to cofactor perturbations in Escherichia coli. J. Biol. Chem. 285, 17498–17506.

Ho, S.-H., Chen, C.-Y., Chang, J.-S., 2012. Effect of light intensity and nitrogen starvation on CO2 fixation and lipid/carbohydrate production of an indigenous microalga Scenedesmus obliquus. CNW-N. Bioresour. Technol. 113, 244–252.

Huckauf, J., Nomura, C., Forchhammer, K., Hagemann, M., 2000. Stress responses of Synechocystis sp. strain PCC 6803 mutants impaired in genes encoding putative alternative sigma factors. Microbiology 146 (Pt 11), 2877–2889.

Ito, S., Koyama, N., Osanai, T., 2019. Citrate synthase from Synechocystis is a distinct class of bacterial citrate synthase. Sci. Rep. 9 (1), 6038. https://doi.org/10.1038/s41598-019-42659-z.

Jahn, M., Vialas, V., Karlsen, J., Maddalo, G., Edfors, F., Forsström, B., Uhlén, M., Käll, L., Hudson, E.P., 2018. Growth of cyanobacteria is constrained by the abundance of light and carbon assimilation proteins. Cell Rep. 25, 478–486 e8.

Jones, P.R., 2014. Genetic instability in cyanobacteria - an elephant in the room? Front Bioeng Biotechnol 2, 12.

Karlsen, J., Asplund-Samuelsson, J., Jahn, M., Vitay, D., Hudson, E.P., 2021. Slow protein turnover explains limited protein-level response to diurnal transcriptional oscillations in cyanobacteria. Front. Microbiol. 12, 1–12. https://doi.org/10.3389/fmicb.2021.657379.

Karlsen, J., Asplund-Samuelsson, J., Thomas, Q., Jahn, M., Hudson, E.P., 2018. Ribosome profiling of synechocystis reveals altered ribosome allocation at carbon starvation. mSystems 3, 1–12. https://doi.org/10.1128/msystems.00126-18.

Koch, M., Berendzen, K.W., Forchhammer, A.K., 2020. On the role and production of polyhydroxybutyrate (PHB) in the cyanobacterium sp. PCC 6803. Life 10. https://doi.org/10.3390/life10040047.

Koch, M., Doello, S., Gutekunst, K., Forchhammer, K., 2019. PHB is produced from glycogen turnover during nitrogen starvation in *Synechocystis sp.* PCC 6803. Intl. J. Mol. Sci. 20, 1942. https://doi.org/10.3390/ijms20081942.

Krasikov, V., Aguirre von Wobeser, E., Dekker, H.L., Huisman, J., Matthijs, H.C.P., 2012. Time-series resolution of gradual nitrogen starvation and its impact on photosynthesis in the cyanobacterium Synechocystis PCC 6803. Physiol. Plantarum 145, 426–439.

Labarre, J., Thuriaux, P., Chauvat, F., 1987. Genetic analysis of amino acid transport in the facultatively heterotrophic cyanobacterium Synechocystis sp. strain 6803. J. Bacteriol. 169, 4668–4673.

Landberg, J., Wright, N.R., Wulff, T., Herrgård, M.J., Nielsen, A.T., 2020. CRISPR interference of nucleotide biosynthesis improves production of a single-domain antibody in Escherichia coli. Biotechnol. Bioeng. 117, 3835–3848.

Li, S., Jendresen, C.B., Grünberger, A., Ronda, C., Jensen, S.I., Noack, S., Nielsen, A.T., 2016. Enhanced protein and biochemical production using CRISPRi-based growth switches. Metab. Eng. 38, 274–284.

Lo, T.-M., Chng, S.H., Teo, W.S., Cho, H.-S., Chang, M.W., 2016. A two-layer gene circuit for decoupling cell growth from metabolite production. Cell Syst 3, 133–143.

Love, M.I., Huber, W., Anders, S., 2014. Moderated estimation of fold change and dispersion for RNA-seq data with DESeq2. Genome Biol. 15, 550.

Lynch, M.D., 2016. Into new territory: improved microbial synthesis through engineering of the essential metabolic network. Curr. Opin. Biotechnol. 38, 106–111.

Marin, K., Kanesaki, Y., Los, D.A., Murata, N., Suzuki, I., Hagemann, M., 2004. Gene expression profiling reflects physiological processes in salt acclimation of Synechocystis sp. strain PCC 6803. Plant Physiol 136, 3290–3300.

Mironov, K.S., Sinetova, M.A., Shumskaya, M., Los, D.A., 2019. Universal Molecular Triggers of Stress Responses in Cyanobacterium Synechocystis. Life. https://doi.org/10.3390/life9030067.

Muro-Pastor, M.I., Reyes, J.C., Florencio, F.J., 2005. Ammonium assimilation in cyanobacteria. Photosynth. Res. 83, 135–150.

Muro-Pastor, M.I., Reyes, J.C., Florencio, F.J., 2001. Cyanobacteria perceive nitrogen status by sensing intracellular 2-oxoglutarate levels. J. Biol. Chem. 276, 38320–38328.

Oliver, J.W.K., Atsumi, S., 2014. Metabolic design for cyanobacterial chemical synthesis. Photosynth. Res. 120, 249–261.

Orf, I., Schwarz, D., Kaplan, A., et al., 2016. CyAbrB2 contributes to the transcriptional regulation of low CO2 acclimation in synechocystis sp. PCC 6803. Plant Cell Physiol. 57 (10), 2232–2243. https://doi.org/10.1093/pcp/pcw146.

Quintero, M.J., Montesinos, M.L., Herrero, A., Flores, E., 2001. Identification of genes encoding amino acid permeases by inactivation of selected ORFs from the Synechocystis genomic sequence. Genome Res. 11, 2034–2040.

Quintero, M.J., Muro-Pastor, A.M., Herrero, A., Flores, E., 2000. Arginine catabolism in the cyanobacterium Synechocystis sp. Strain PCC 6803 involves the urea cycle and arginase pathway. J. Bacteriol. 182, 1008–1015.

Richaud, C., Zabulon, G., Joder, A., Thomas, J.-C., 2001. Nitrogen or sulfur starvation differentially affects phycobilisome degradation and expression of the nblA gene in synechocystis strain PCC 6803. J. Bacteriol. 183, 2989–2994. https://doi.org/10.1128/jb.183.10.2989-2994.2001.

Schneider, D.A., Gaal, T., Gourse, R.L., 2002. NTP-sensing by rRNA promoters in Escherichia coli is direct. Proc. Natl. Acad. Sci. U. S. A. 99 (13), 8602–8607. https://doi.org/10.1073/pnas.132285199.

Schramm, T., Lempp, M., Beuter, D., Sierra, S.G., Glatter, T., Link, H., 2020. High-throughput enrichment of temperature-sensitive argininosuccinate synthetase for two-stage citrulline production in E. coli. Metab. Eng. 60, 14–24.

Schwarz, R., Forchhammer, K., 2005. Acclimation of unicellular cyanobacteria to macronutrient deficiency: emergence of a complex network of cellular responses. Microbiology 151, 2503–2514.

Searle, B.C., Pino, L.K., Egertson, J.D., Ting, Y.S., Lawrence, R.T., MacLean, B.X., Villén, J., MacCoss, M.J., 2018. Chromatogram libraries improve peptide detection and quantification by data independent acquisition mass spectrometry. Nat. Commun. 9, 5128.

Shabestary, K., Anfelt, J., Ljungqvist, E., Jahn, M., Yao, L., Hudson, E.P., 2018. Targeted repression of essential genes to arrest growth and increase carbon partitioning and biofuel titers in cyanobacteria. ACS Synth. Biol. 7, 1669–1675.

Shabestary, K., Hudson, E.P., 2016. Computational metabolic engineering strategies for growth-coupled biofuel production by. Metab Eng Commun 3, 216–226.

Solomon, K.V., Sanders, T.M., Prather, K.L.J., 2012. A dynamic metabolite valve for the control of central carbon metabolism. Metab. Eng. 14, 661–671.

Soma, Y., Tsurunom, K., Wada, M., Yokota, A., Hanai, T., 2014. Metabolic flux redirection from a central metabolic pathway toward a synthetic pathway using a metabolic toggle switch. Metab. Eng. 23, 175–184.

van Alphen, P., Hellingwerf, K.J., 2015. Sustained circadian rhythms in continuous light in synechocystis sp. PCC6803 growing in a well-controlled photobioreactor. PLoS One 10, e0127715.

Vavilin, D.V., Vermaas, W.F.J., 2002. Regulation of the tetrapyrrole biosynthetic pathway leading to heme and chlorophyll in plants and cyanobacteria. Physiol. Plantarum 115, 9–24.

Vázquez-Bermúdez, M.F., Herrero, A., Flores, E., 2000. Uptake of 2-oxoglutarate in Synechococcus strains transformed with the Escherichia coli kgtP gene. J. Bacteriol. 182, 211–215.

Venayak, N., Anesiadis, N., Cluett, W.R., Mahadevan, R., 2015. Engineering metabolism through dynamic control. Curr. Opin. Biotechnol. 34, 142–152.

Wang, H.L., Postier, B.L., Burnap, R.L., 2004. Alterations in global patterns of gene expression in Synechocystis sp. PCC 6803 in response to inorganic carbon limitation and the inactivation of ndhR, a LysR family regulator. J. Biol. Chem. 279 (7), 5739–5751. https://doi.org/10.1074/jbc.M311336200.

Wu, P., Chen, Y., Liu, M., Xiao, G., Yuan, J., 2021. Engineering an optogenetic CRISPRi platform for improved chemical production. ACS Synth. Biol. 10, 125–131.

Yao, L., Shabestary, K., Björk, S.M., Asplund-Samuelsson, J., Joensson, H.N., Jahn, M., Hudson, E.P., 2020. Pooled CRISPRi screening of the cyanobacterium Synechocystis sp PCC 6803 for enhanced industrial phenotypes. Nat. Commun. 11, 1666.

Young, J.D., Shastri, A.A., Stephanopoulos, G., Morgan, J.A., 2011. Mapping photoautotrophic metabolism with isotopically nonstationary (13)C flux analysis. Metab. Eng. 13 (6), 656–665. https://doi.org/10.1016/j.ymben.2011.08.002.

Zavřel, T., Faizi, M., Loureiro, C., Poschmann, G., Stühler, K., Sinetova, M., Zorina, A., Steuer, R., Červený, J., 2019. Quantitative insights into the cyanobacterial cell economy. Elife 8. https://doi.org/10.7554/eLife.42508.

Zhang, Z., Pendse, N.D., Phillips, K.N., Cotner, J.B., Khodursky, A., 2008. Gene expression patterns of sulfur starvation in Synechocystis sp. PCC 6803. BMC Genom. 9, 344.

Zhou, J., Zhang, F., Meng, H., Zhang, Y., Li, Y., 2016. Introducing extra NADPH consumption ability significantly increases the photosynthetic efficiency and biomass production of cyanobacteria. Metab. Eng. 38, 217–227.